Обзор ArXiv/astro-ph, 16 сентября 2021 года

От Сильченко О.К.

ArXiv: 2109.06197

From large-scale environment to CGM angular momentum to star forming activities – II: quenched galaxies

Shengdong Lu[1]★, Dandan Xu[1]†, Sen Wang[1], Zheng Cai[1], Chuan He[2,3,4], C. Kevin Xu[2,4], Xiaoyang Xia[5], Shude Mao[1,2], Volker Springel[6], Lars Hernquist[7]

[1]*Department of Astronomy, Tsinghua University, Beijing 100084, China*
[2]*National Astronomical Observatories, Chinese Academy of Sciences, Beijing 100101, China*
[3]*School of Astronomy and Space Sciences, University of Chinese Academy of Sciences, Beijing 100049, China*
[4]*Chinese Academy of Sciences South America Center for Astronomy, Beijing 100101, China*
[5]*Tianjin Astrophysics Center, Tianjin Normal University, Tianjin 300387, China*
[6]*Max-Planck-Institut für Astrophysik, Karl-Schwarzschild-Str. 1, D-85748, Garching, Germany*
[7]*Harvard-Smithsonian Center for Astrophysics, 60 Garden Street, Cambridge, MA 02138, USA*

Accepted ***. Received ***; in original form ***

ABSTRACT

The gas needed to sustain star formation in galaxies is supplied by the circumgalactic medium (CGM), which in turn is affected by accretion from large scales. In a series of two papers, we examine the interplay between a galaxy's ambient CGM and central star formation within the context of the large-scale environment. We use the IllustrisTNG-100 simulation to show that the influence exerted by the large-scale galaxy environment on the CGM gas angular momentum results in either enhanced (Paper I) or suppressed (Paper II, this paper) star formation inside a galaxy. We find that for present-day quenched galaxies, both the

IllustrisTNG-100: центральные галактики групп

General properties of the simulated galaxies are taken from the TNG public catalogue (Nelson et al. 2019a). In addition, we also carry out calculations for a number of other key properties related to the galaxy itself, its CGM and its environmental angular momentum. To do so, we first define the galaxy domain as the region inside twice the half-stellar-mass radius $R_{\rm hsm}$ from the galaxy centre; and the region outside $2R_{\rm hsm}$ as the CGM domain (DeFelippis et al. 2020). The relevant properties inside the galaxy domain include a galaxy's specific star formation rate (sSFR), central gas fraction $f_{\rm gas,<2R_{hsm}}$, and specific gaseous and stellar disk spin vectors $\mathbf{j}_{\rm gas}$ and $\mathbf{j}_*$, respectively. $\mathbf{j}_{\rm gas}$ and $\mathbf{j}_*$ are calculated as:

$$\mathbf{j}_x = \frac{\sum_i m_i \mathbf{r_i} \times \mathbf{v_i}}{\sum_i m_i}, \quad (1)$$

where the subscript x refers to stars or gas inside the galaxy domain; m_i, $\mathbf{r_i}$ and $\mathbf{v_i}$, respectively, are the mass, position and velocity vectors with respect to the galaxy centre, of the i-th stellar/gaseous element. The summation goes over all the stellar/gaseous particles/cells within $2R_{\rm hsm}$. We refer the reader to Lu et al. (2021) and Xu et al. (2019)

In order to eliminate the effects of mass dependence, we also define a dimensionless spin for the CGM around each galaxy as follows:

$$\lambda_{\rm CGM} = \sum_i \frac{m_i\, v_{{\rm t},i}^2}{GM(\leqslant r_i)/r_i} \Big/ \sum_i m_i, \quad (2)$$

where m_i, r_i and $v_{{\rm t},i}$, respectively, are the mass, distance and tangential velocity of the i-th gas element with respect to the galaxy centre, G is the gravitational constant, and $M(\leqslant r_i)$ is the total mass enclosed within distance r_i. To evaluate and compare among different galaxy types the spin of the CGM as a whole, the summation is over all gas elements within a fixed radial range of 30-300 kpc from the galaxy centre. We note that the dimensionless spin defined in this way is different from the conventional definition (e.g., Stewart et al. 2011, 2017; Teklu et al. 2015; Danovich et al. 2015), which is essentially a globally-defined angular momentum ratio evaluated within a certain radius. The definition used here is a mass-weighted energy fraction of the tangential motion with respect to the total kinetic energy that is required to balance gravity at this radius (assuming a

- Три бина по радиусу: R<2Re галактика, R>2Re(газ) – CGM, R до 200 кпк (спутники) – окружение
- Для каждого компонента считается суммарный момент (вектор)
- А для окологалактической среды – еще и спин (число)

Газа и момента больше у массивных галактик;

но при фиксированной массе момента (CGM) больше у «спокойных» галактик

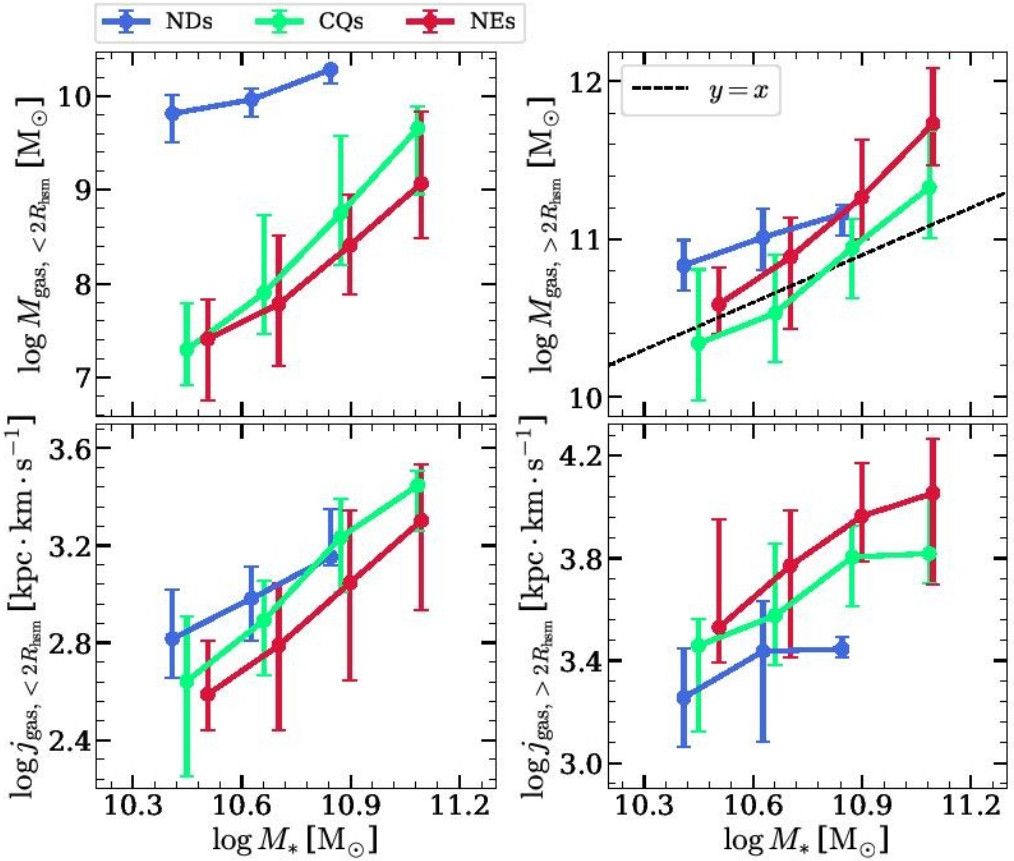

Figure 1. Left: the distributions of mass (top) and specific spin (bottom) of inner ($r < 2R_{\rm hsm}$) gas, as a function of galaxy stellar mass M_*, in c galaxies (green), normal elliptical galaxies (red), and normal disk galaxies (blue). Right: the same plots for the outer gas ($r > 2R_{\rm hsm}$, also define

А среди галактик со звездообразованием…

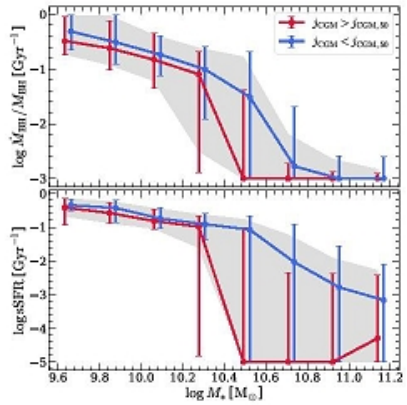

Figure 2. The distributions of the black hole accretion rate $\dot{M}_{BH}/M_{BH}$ (top panel) and the specific star-formation rate sSFR within $2R_{b50}$ (bottom panel) as a function of galaxy stellar mass M_* for all the three types of galaxies (i.e. NDs, CQs, and NEs) and their progenitors since $z = 1$. In each panel, galaxies are divided into 8 bins according to their stellar masses, with the grey shaded region indicating the $\pm 1\sigma$ region of all the galaxies. In each bin, galaxies are further divided into two subgroups according to their CGM angular momenta j_{CGM}; i.e., galaxies with $j_{CGM} > j_{CGM,50}$ (red) and with $j_{CGM} < j_{CGM,50}$ (blue), where $j_{CGM,50}$ is the median j_{CGM} in each stellar mass bin. The error bars indicate the range from 16th to 84th percentiles ($\pm 1\sigma$).

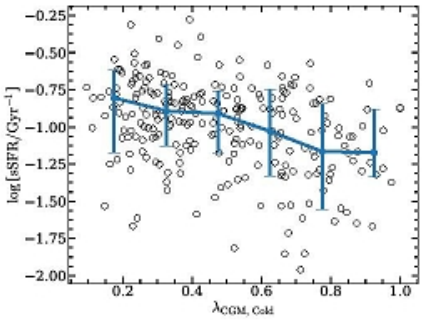

Figure 3. The distribution of the logarithmic sSFR as a function of dimensionless spin λ_{CGM} of the cold CGM gas (i.e., with 10^4 K $< T < 2 \times 10^4$ K, and located within a radial range of 30 – 100 kpc) for star-forming disk galaxies at $z \leqslant 0.1$. The solid line connects the median values in λ_{CGM} bins; the error bars indicate the ranges from 16th to 84th percentiles ($\pm 1\sigma$) of the distribution.

- Есть антикорреляция удельных темпов звездообразования со спином окологалактической среды

Совсем много спина CGM у галактик БЕЗ звездообразования

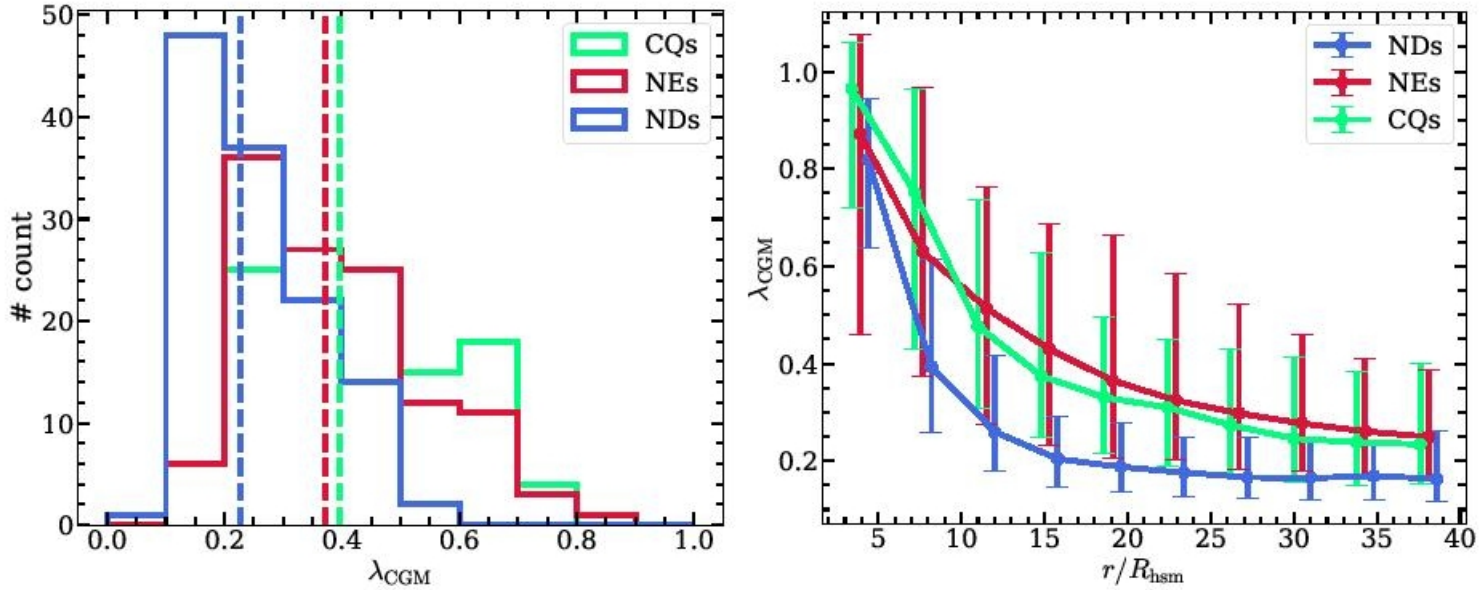

Figure 5. Left: histograms of the CGM dimensionless spin $\lambda_{\rm CGM}$ (evaluated within a radial range of 30 – 300 kpc, see Eq. 2 for definition) for three types of galaxies at $z = 0$. The dashed line indicates the median value in each case. Right: radial profiles of the CGM dimensionless spin $\lambda_{\rm CGM}$ for the same galaxy samples. The error bars indicate the ranges from 16th to 84th percentiles ($\pm 1\sigma$) in individual cases.

Двигают идею, что момент в CGM приходит от спутников; но со взаимными ориентациями момента – загадка…

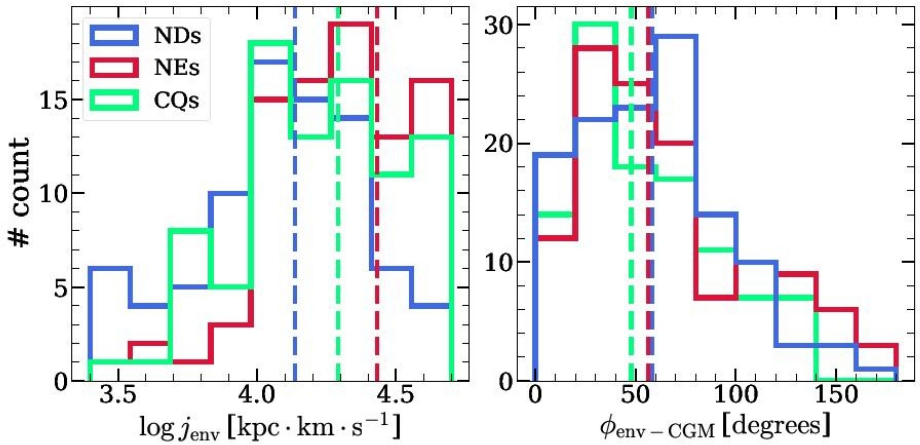

Figure 6. Histograms of the specific environmental angular momentum $j_{\rm env}$ (left panel; evaluated in the distance range of 50 – 300 kpc from the host galaxy; see Eq. 3 for definition) and of misalignment angles between $\mathbf{j}_{\rm CGM}$ and $\mathbf{j}_{\rm env}$ (right panel), for NDs (blue), CQs (green), and NEs (red) selected at $z = 0$. In each panel, the dashed lines indicate the median values of the investigated parameters for the three types of galaxies.

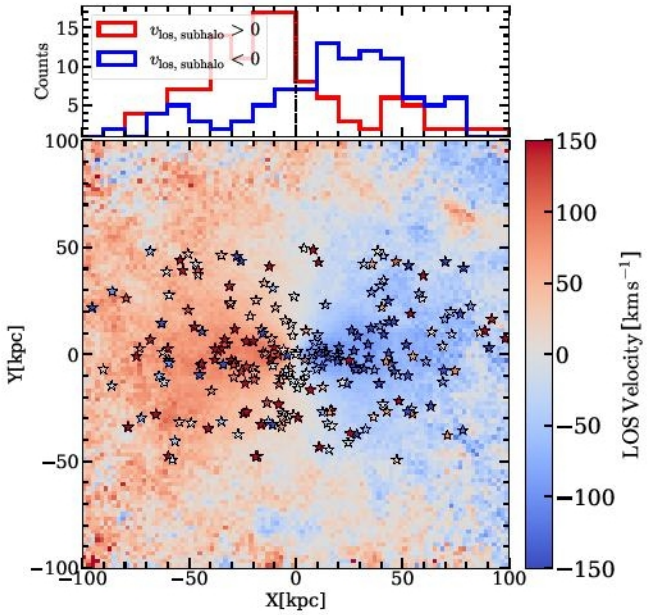

Figure 8. Stacked line-of-sight velocity fields of all the star-forming disks and the quenched but dynamically cold early-type galaxies at $z = 0$. Before stacking, all the galaxies are rotated to edge-on views according to their stellar disks such that the galaxy major axes are along the X-axis in the figure. A further rotation with a random disk inclination angle between $-60°$ and $60°$ along the major axis is then applied to each galaxy, in order to mimic a nearly edge-on view from an observation. The color-coded maps present the stacked signal of the line-of-sight velocity fields of the cold (10^4 K $< T < 2\times10^4$ K) CGM gas. The star symbols with colors indicate the line-of-sight velocities of galaxies (with projected $|Y| < 50$ kpc) in the vicinity of the hosts. The

Эволюция момента

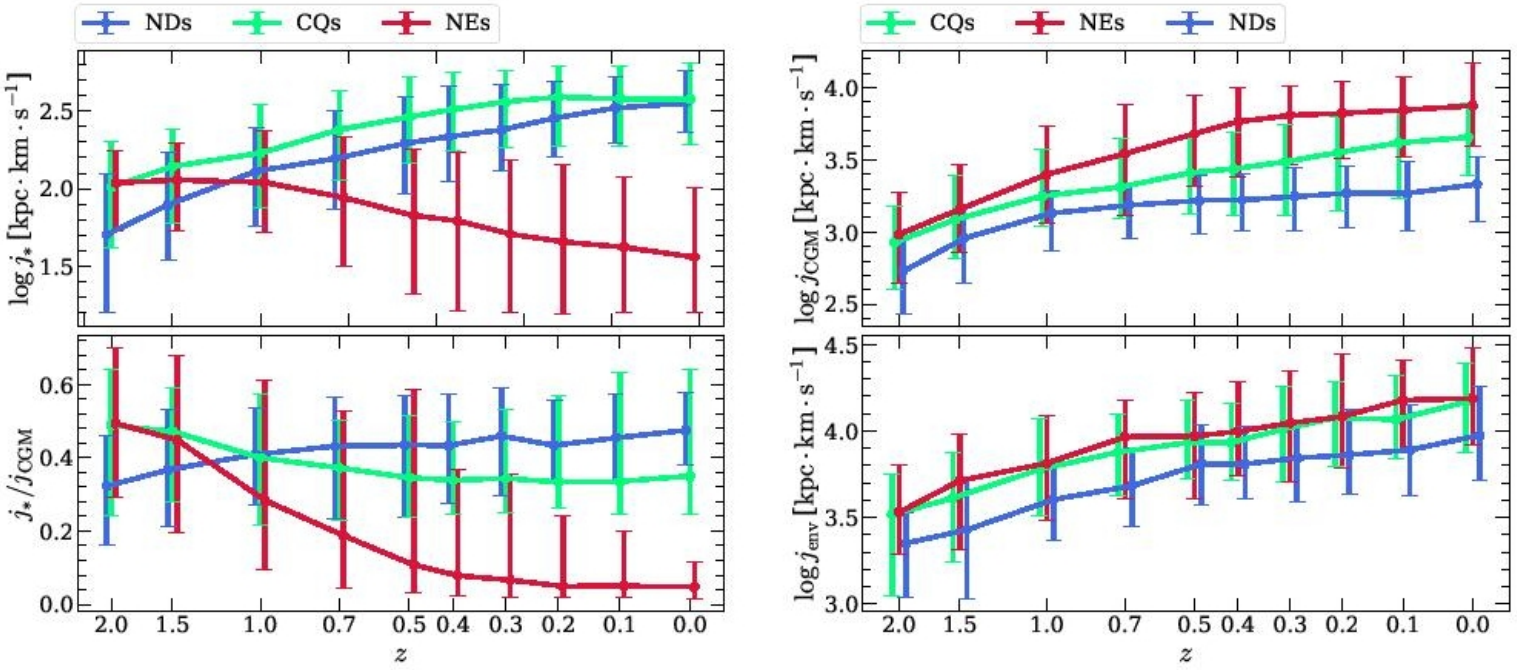

Figure 7. The redshift evolution of: **(1)** the stellar spin within $2R_{hsm}$ (log j_*, top left), **(2)** the specific CGM gas angular momentum (log j_{CGM}, top right; evaluated at $r > 2R_{hsm}$, see Eq. 1 for definition), **(3)** the ratio between the two angular momenta above (i.e., j_*/j_{CGM}, bottom left), and **(4)** the specific environmental angular momentum (log j_{env}, bottom right; see Eq. 3 for definition). In each panel, CQs, NEs, and NDs are indicated by green, red, and blue lines, with error bars indicating the range from the 16th to the 84th percentiles ($\pm 1\sigma$).

Просят поискать антикорреляцию момента со звездообразованием в наблюдениях пар галактик

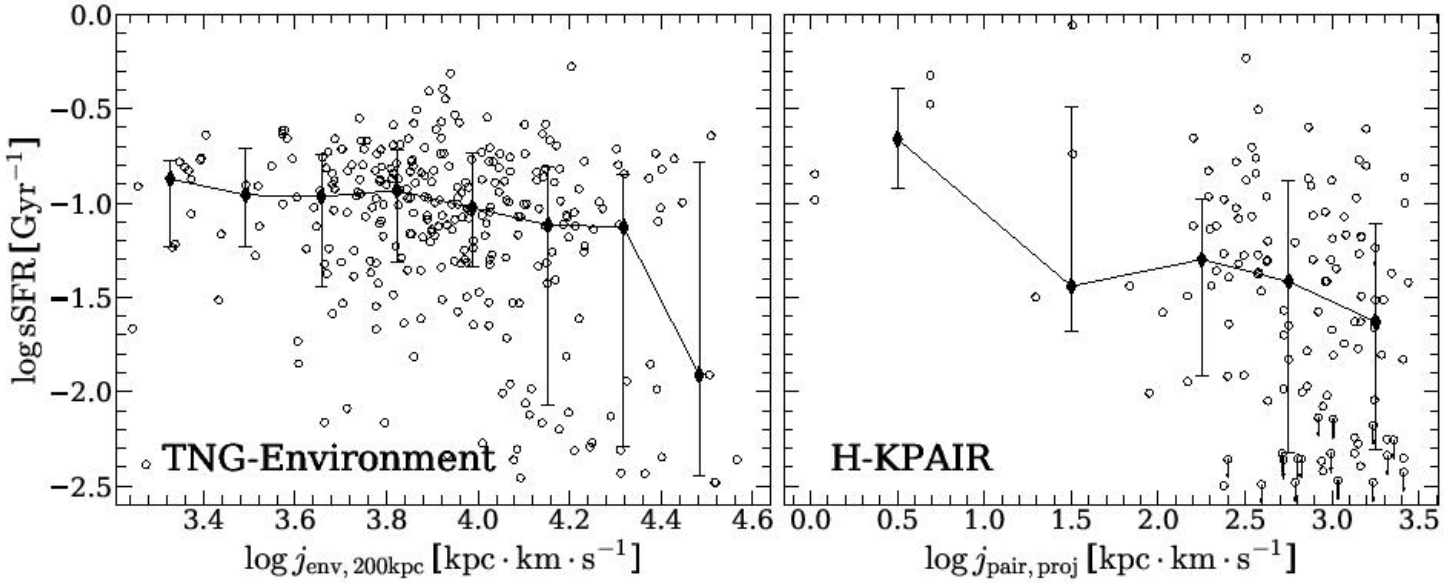

Figure 9. Left: correlation between the specific star-formation rate (log sSFR) and the environmental angular momentum (log $j_{\rm env,200kpc}$, evaluated within 200kpc from the primary galaxy; see Eq. 3 for definition) of the TNG galaxy samples at $z \leqslant 0.1$ (the same redshift range as the H-KPAIR sample on the right). The median profile of log sSFR as a function of log $j_{\rm env,200kpc}$ is indicated by the black lines. Right: correlation between the specific star-formation rate (log sSFR) and the angular momenta of galaxy pairs (log $j_{\rm pair,proj}$, see Eq. 4 for definition) in the H-KPAIR sample. The error bars in both panels indicate the ranges from 16th to 84th percentiles ($\pm 1\sigma$).

Без омоложения модель не получается?

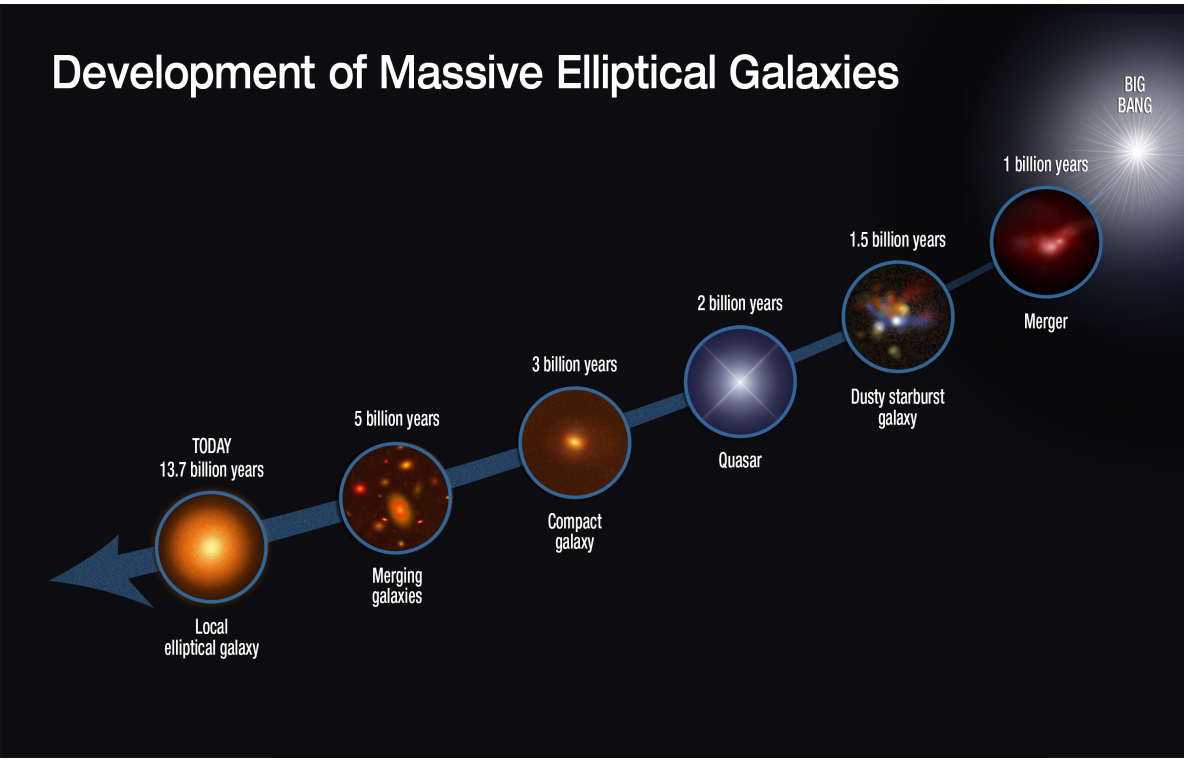

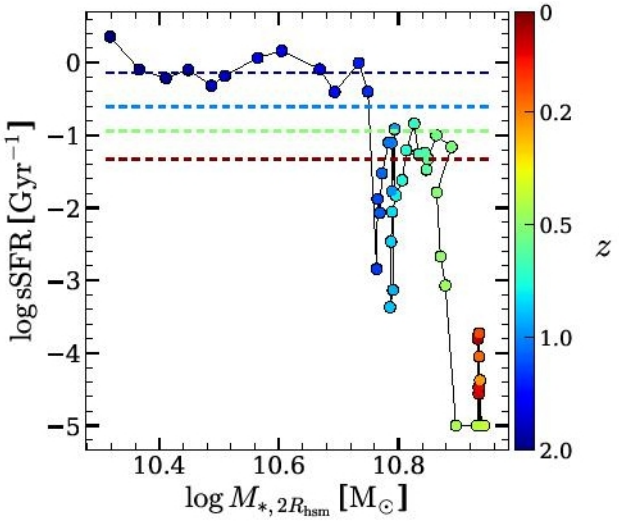

Figure 10. The redshift evolution in the log sSFR − log M_* plane for a present-day quenched elliptical galaxy (ID: 407204). Four dashed lines from top to bottom indicate the lower boundary in log sSFR for the main sequence galaxies at z = 2, 1, 0.5, 0 (indicated by colors), below which galaxies are regarded as quenched. The lower boundary is calculated as the 16th percentile of the sSFR for the galaxies with $10^{9.5}$M$_\odot$ $\leqslant$ M_* $\leqslant$ $10^{10.5}$M$_\odot$ at different redshifts.

ArXiv: 2107.09528

SDSS-IV MaNGA: Kinematics and stellar population of a complete sample of galaxies with counter-rotating stellar disks selected from about 4000 galaxies

Davide Bevacqua,[1⋆] Michele Cappellari,[2] Silvia Pellegrini[1,3]
[1] *Department of Physics and Astronomy, University of Bologna, via P. Gobetti 93/2, 40129 Bologna, Italy*
[2] *Sub-department of Astrophysics, Department of Physics, University of Oxford, Denys Wilkinson Building, Keble Road, Oxford, OX1 3RH, UK*
[3] *INAF-OAS of Bologna, via P. Gobetti 93/3, 40129 Bologna, Italy*

Accepted XXX. Received YYY; in original form ZZZ

ABSTRACT

We present the kinematics and stellar population properties of a sample of 53 galaxies (50 are Early-Type galaxies, ETGs) with Counter-Rotating Disks (CRD) extracted from a sample of about 4000 galaxies of all morphological types in the MaNGA survey (DR16). The kinematic maps were used to select galaxies based on evidence of counter-rotation in the velocity maps or two peaks in the velocity dispersion maps. For about 1/3 of the sample, the counter-rotating components can also be separated spectroscopically. We then produced the age and metallicity maps, and compared the stellar population properties to those of the general ETGs population. We found that CRDs have similar trends in age and metallicity, but they are generally less metallic at low masses. The metallicity gradients are similar; instead, age gradients are typically flatter and confined within a smaller range of values. We compared the velocity fields of the ionized gas and the stars, and found that in 25 cases the gas corotates with either the inner (13 cases) or the outer (12 cases) disk, and in 9 cases the gaseous and stellar disks are misaligned. With one exception, all misaligned cases have stellar masses less than $3 \times 10^{10} M_{\odot}$. We also compared stellar and gaseous disks with age maps and found that in most cases the gas corotates with the younger disk. We looked for evidences of multimodality in the stellar

Выборка: 4000(DR16)→53 CR(?)

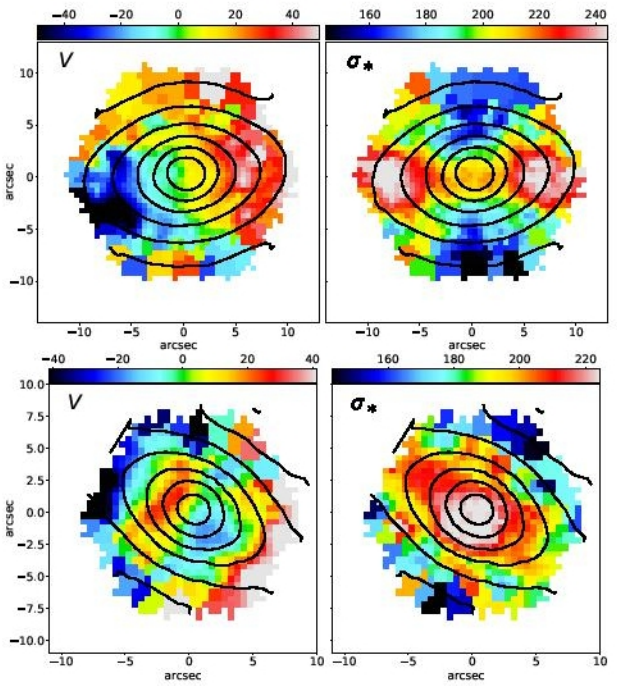

Figure 2. Velocity, V, and velocity dispersion, σ_*, maps of two galaxies, one (upper panels) exhibiting the characteristic two peaks in σ_* but no counter-rotation, and the other (lower panels) exhibiting counter-rotation, but a single central peak in σ_*.

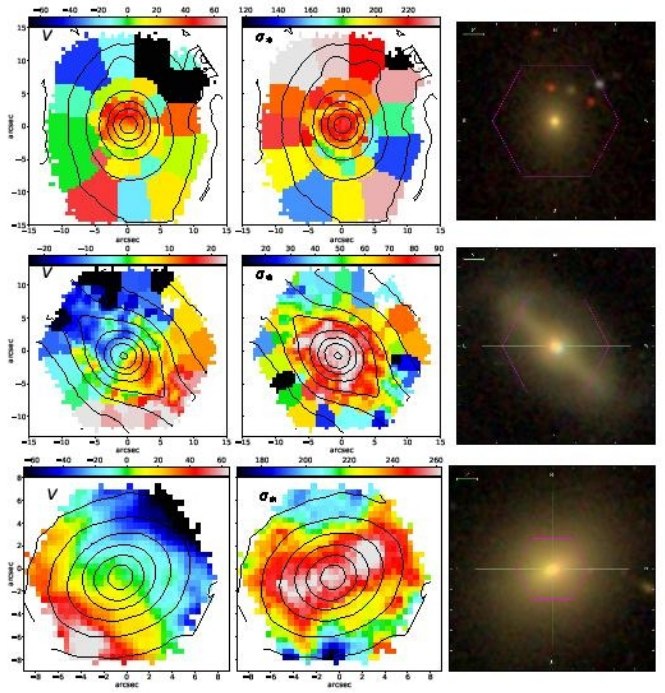

Figure 3. Velocity map, velocity dispersion map and SDSS image of three galaxies with kinematic features resembling those of CRD while not truly being so. Colorbars are in km s^{-1}. Black lines are the flux contours. *First row:* in the velocity map an inversion of rotation is seen in the northern region, but from the SDSS image it is evident that kinematic maps are defaced by the presence of external objects. *Second and third rows:* the dispersion maps present two elongated peaks: the presence of a bar is revealed by

Потому что лень все просматривать…

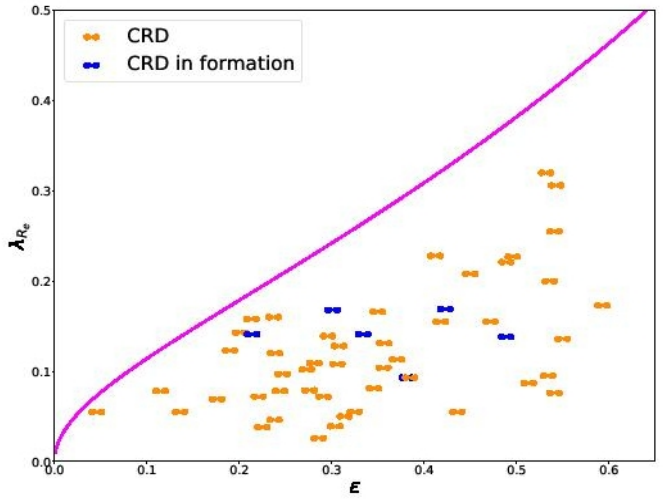

Figure 4. Final sample of CRDs plotted on the $(\lambda_{R_e}, \varepsilon)$ diagram. The magenta line is the same of Figure 1. Galaxies labelled as 'CRD in formation' have a bluish and/or irregular SDSS image.

- В результате соотношение морфологических типов галактик с противовращением звездных дисков (E:S0:Sp=34:16:3) не отражает реальность (скорее всего)

Низкое S/N → примитивный фит → 15 галактик с разделившимися дисками

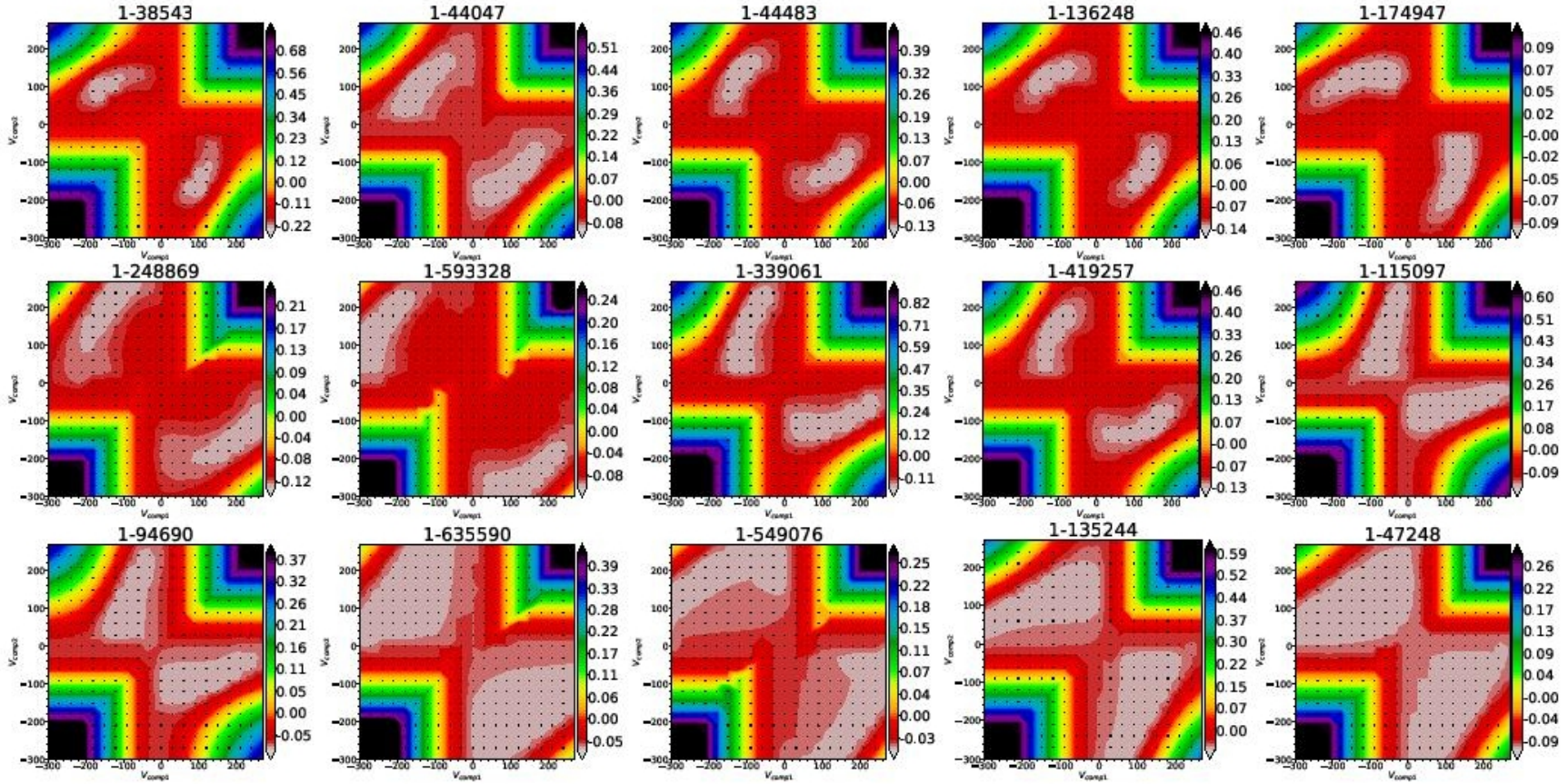

Figure 9. χ^2 maps of CRDs exhibiting two distinct minima, namely those where the two kinematic components are spectroscopically distinguishable. These maps were obtained by fitting a single representative spectrum per galaxy, chosen at one of the two σ peaks, where the separation between the components is the largest (appendix B). MaNGA-IDs are plotted above each panels. Colorbars values are the $\log_{10}(\chi^2/\mathrm{DOF})$. In each panel, the x and y axes are the fitted V_{comp1} and V_{comp2}, ranging within ± 300 km s^{-1} at $V_{\mathrm{step}} = 30$ km s^{-1}.

Сопоставление с возрастом (и металличностью) дисков

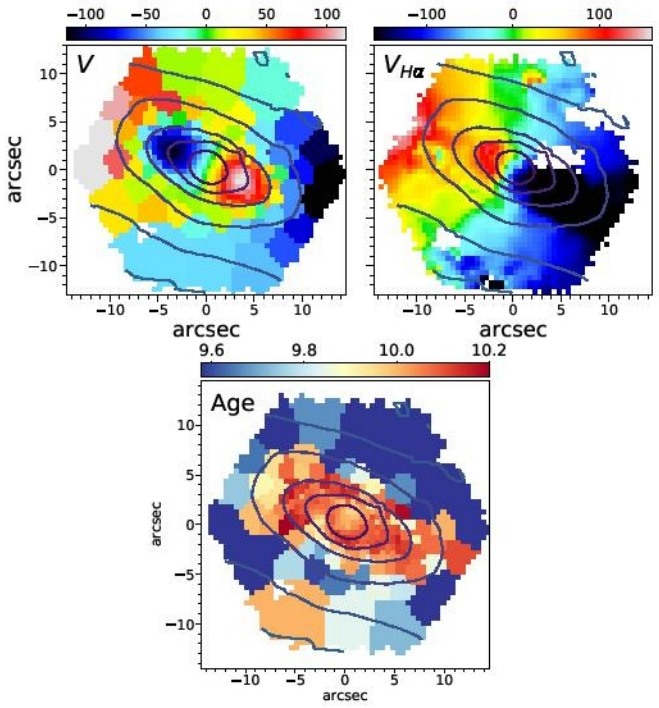

Figure 7. Stellar and gas velocity maps (upper panels) compared to the logarithmic age map (lower panel) of a CRD. Velocities are in km s^{-1}. Age values are calculated using equation (4). In this example, we can see an abrupt change in age, coinciding with the inversion of the stellar rotation. The stellar rotation is inverted halfway from the third to the fourth isophote, starting from the center.The outer disk, which is corotating with the ionised gas, is

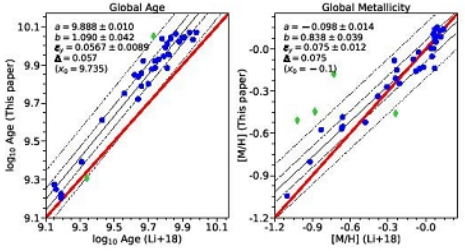

Figure 11. Comparison of global age and metallicity for 36 CRDs in common with the sample of Li+18. The blue dots are the values used to fit the linear relation $y = a + b(x - x_0)$, with x_0 being the mean value, while green dots are outliers excluded by the routine during the fit. The black dashed and dotted lines are the 1σ and 2.6σ confidences, respectively. The red straight line is the $y = x$ line. The best-fit coefficients are texted on the plots; ε_y and Δ are the intrinsic and observed scatters, respectively.

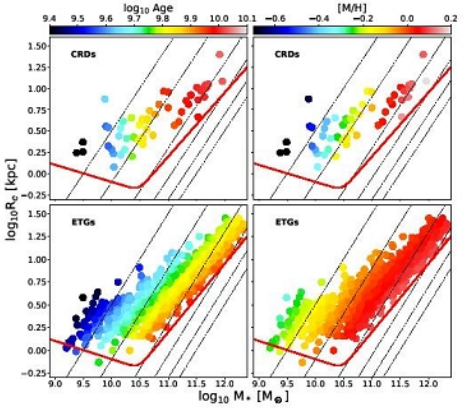

Figure 12. LOESS-smoothed $\log_{10}$Age (left columns) and metallicity [M/H] (right columns) of CRDs (upper panels) and ETGs from Li+18 (lower panels). Lines are the same of Figure 10. Note: masses of CRDs are calculated from the photometry, using equation (2) of Cappellari (2013); instead, masses in Li+18 are calcu-

Звезды vs ионизованный газ

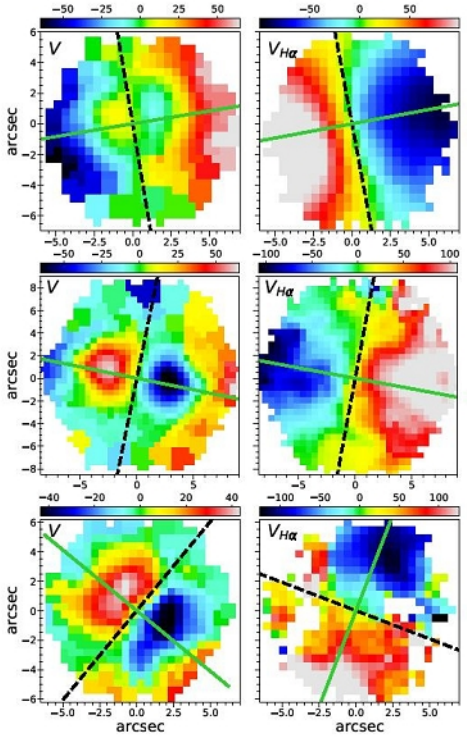

Figure 6. Three representative examples of stars (left columns) and gas (right columns) velocity fields of galaxies with the gaseous disk corotating with the inner disk (upper panels), with the outer disk (middle panels) and misaligned (lower panels). The straight lines in green are the major axis PAs, and the black dashed lines mark the rotation axes (calculated as PA+90°). Colorbars are the velocity ranges in km s^{-1}.

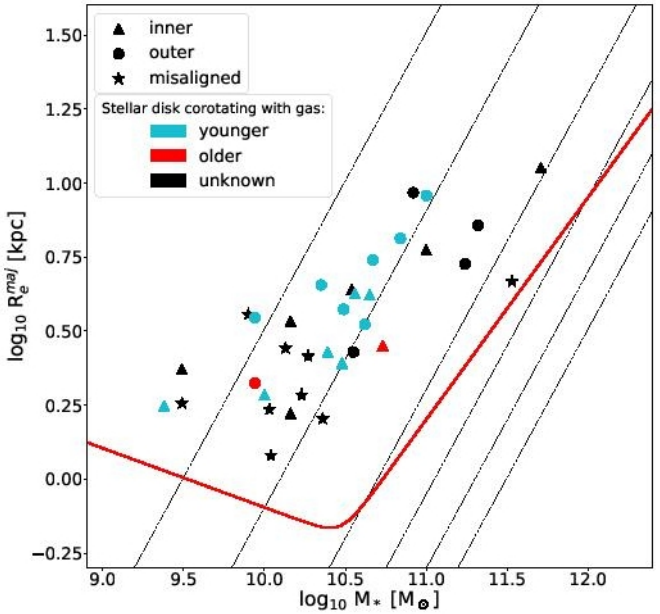

Figure 10. Alignment of the ionised gas with respect to the stellar rotation on the mass-size plane of CRDs. Here, M_* is the stellar mass, and $R_e^{maj} = 1.61 \times R_e$ is the effective radius of the major axis, defined in Cappellari et al. (2013a). The dashed black lines are lines of constant velocity dispersion at (left to right) 50, 100, 200, 300, 400, 500 km s^{-1}. The red straight line is the zone of exclusion, defined in Cappellari et al. (2013a). The labels 'inner' and 'outer' refer, respectively, to the corotation of the gas with the stellar disk prevailing the inner or outer regions of the velocity

Попытка разделить два компонента по возрасту – регуляризация из последних сил

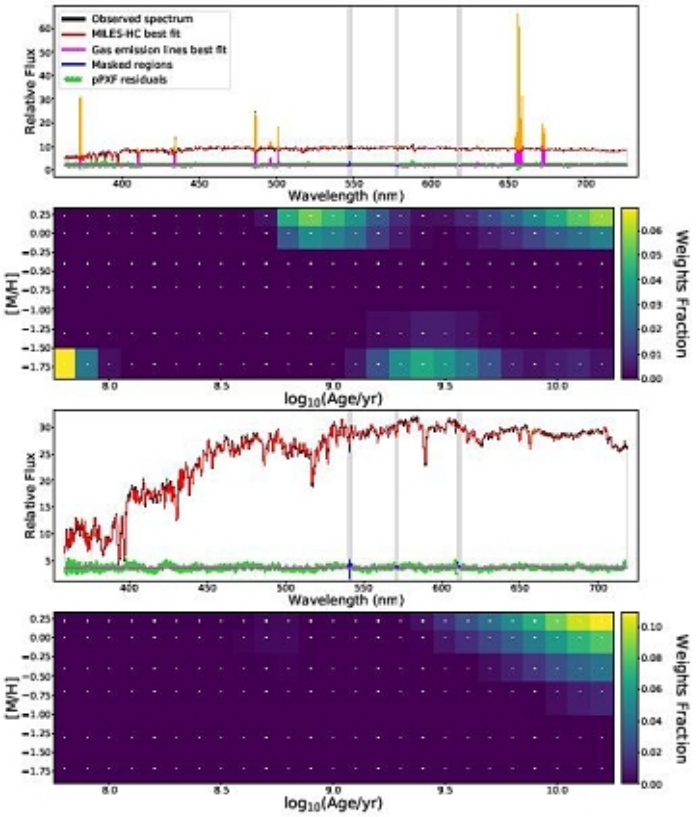

Figure 8. Examples of multimodal and unimodal maps. The two upper panels show the stellar population fit and the weights fraction map of the SSPs of a central spatial bin of a galaxy with multiple populations. The two lower panels, instead, are the fit and the weights map of a central spatial bin of a galaxy with a single population.

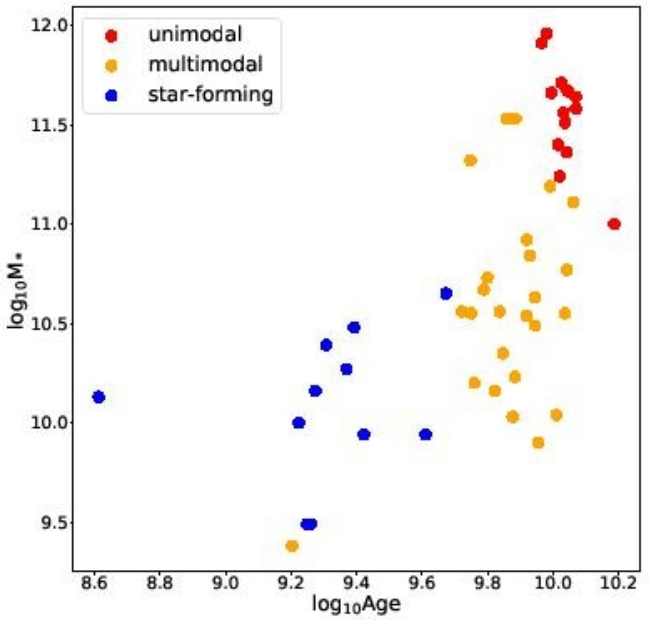

Figure 14. CRDs on the mass vs. age diagram. The distinction into unimodal, multimodal and star-forming is based on the weights maps of regularised fits (section 4.3) and was possible for 49 CRDs. Unimodal and multimodal galaxies are those exhibiting the same single or multiple blobs all over the galaxy, while those labelled as star-forming have multimodal maps that change at different spatial regions of the galaxy.

Выводы: сценариев много

- Собственно, только 15 случаев, где противовращение проявляется в LOSVD
- Если смотреть возраст на разных радиусах – то чаще всего газ лежит в плоскости и вращается вместе с более молодым из звездных дисков; это аккреция ретроградного газа.
- Но есть и 2 случая, когда вместе с более старым – такой большой мержинг?
- Диски с двумя компонентами, разными по возрасту, всегда интегрально старые – это уж точно ранний большой мержинг? (так в тексте; но на предыдущей картинке я вижу противоречие…)
- Вывод: противовращающиеся звездные диски могут формироваться разными путями.
- Второй вывод: данные так себе…